Astron. Astrophys. 72, 270–276 (1979)

ASTRONOMY AND ASTROPHYSICS

Radio Continuum Observations at 1420 MHz of the New SNR G65.2+5.7 in Cygnus

W. Reich[1], E. M. Berkhuijsen[2], and Y. Sofue[2]*

[1] Radioastronomisches Institut der Universität Bonn, D-5300 Bonn, Federal Republic of Germany
[2] Max-Planck-Institut für Radioastronomie, Auf dem Hügel 69, D-5300 Bonn 1, Federal Republic of Germany

Received May 17, 1978

Summary. Radio continuum observations at 1420 MHz of the optical SNR discovered by Gull et al. (1977) are presented. Intense radio ridges appear to coincide with bright optical filaments. Observed and derived parameters are collected in Table 4. The main characteristics of this SNR are: diameter ~ 75 pc, distance ~ 0.9 kpc, expansion velocity $\gtrsim 50$ km s^{-1}, age $\lesssim 2.4\ 10^5$ yr, and total kinetic energy $\sim 13\ 10^{51}$ erg. A short comparison with other SNRs is made.

Key words: dynamical model – radio continuum observations – spectral index – supernova remnants

1. Introduction

Recently Gull et al. (1977) have reported the detection of a filamentary loop structure in optical emission lines centred at $(\alpha, \delta)_{1950} = (19^h31^m, +31°10')$, or $(\ell, b) = (65.°6, +6°)$. It is especially bright in [O III] and looks like a supernova remnant (SNR) of large angular extent ($=4° \times 3.°3$). One of the brightest filaments has previously been catalogued by Sharpless (1959) as the H II region S91. Sabbadin and D'Odorico (1976) have shown that the emission line ratios of Hα, [N II] and [S II] in S91 indicate that this filament is part of a SNR. Applying the relations of Daltabuit et al. (1976) between line ratios, linear diameter and expansion velocity of SNRs to S91 they derived a linear diameter $\simeq 34$ pc, distance $\simeq 0.7$ kpc, expansion velocity > 100 km s^{-1} and average density in the filament $\simeq 450$ cm^{-3}. Both Sabbadin and D'Odorico as well as Gull et al. found some evidence of radio emission at 820 MHz on the map of Berkhuijsen (1972); Sabbadin and D'Odorico found the radio emission to be more apparent on the 408 MHz map of Haslam et al. (1974). Using the surface brightness-linear diameter relation Gull et al. estimated that the SNR has a diameter $\simeq 70$ pc, distance $\simeq 1.2$ kpc, expansion velocity $\gtrsim 50$ km s^{-1}, ambient density $\simeq 0.5$ cm^{-3}, and age $\simeq 3\ 10^5$ yr.

In this paper we present new radio continuum data of the area at 1420 MHz with an angular resolution of 11′. The observations and the reduction procedure are described in Sect. 2; point sources in the area are discussed in Sect. 3; a comparison of the 1420 MHz map and the optical structure is made in Sect. 4, while in Sect. 5 the 1420 MHz data are compared with data at 408 MHz; in Section 6 the surface brightness-linear diameter ($\Sigma - D$) relation and a dynamical model are applied to the new SNR; a summary and a discussion are given in Sect. 7.

Send offprint requests to: E. M. Berkhuijsen
* Senior Humboldt Fellow; on leave from Department of Physics, Nagoya University, Nagoya, Japan

2. Observations and Reductions

The observations were made with the 100-m telescope in Effelsberg of the Max-Planck-Institut für Radioastronomie in April 1977. At 1420 MHz the half-power beamwidth is 9′. The one-channel Dicke receiver switched against a load cooled in liquid helium; a digital back-end with 4 phases was used. The effective bandwidth after rejection of the H I-line band was 18 MHz; the system temperature was 70 K.

The area $\alpha = 19^h20^m$ to 19^h40^m, $\delta = 29.°0$ to $33.°5$ was scanned in δ at a rate of 4.°5/min at intervals of 16^s in α. In order to eliminate possible polarisation effects the measurements were done on 2 consecutive days at the same sidereal time but with orthogonal feed positions.

The standard reduction procedure of Neidhöfer et al. (1978) was used. A second order polynomial was fitted perpendicular to the scan direction through the average of the data points of the outermost 20′ of each scan. The best fits on either side were then used to determine linear baselines for the scans. In this procedure point sources were disregarded. All scans were checked for interference and, if necessary, corrected. Finally the two maps were added and slightly smoothed with a gaussian to a half-power beamwidth of 11′ in order to improve the signal-to-noise ratio. The resulting map is shown in Figs. 1 and 2; the r.m.s. noise is 30 mK in T_b. Features on the map are discussed in Sect. 4.

The source 3C 345 was used as a primary calibrator for which a flux density $S = 6.8 \pm 0.4$ Jy was adopted (Genzel et al., 1976). The source 4C 33.48 ≡ OV + 337 ≡ DA 480, on the border of our map, served as a secondary calibrator; the observed flux density of 3.55 ± 0.05 Jy (standard error only; ± 0.25 Jy if the systematic scale error is included) is in good agreement with other available data (see Table 1). These calibrations yielded $T_b = (1.9 \pm 0.1)\ S$ for the main beam brightness temperature at 11′ resolution. The beam efficiency is 0.70 ± 0.04; the aperture efficiency is 0.53 (Internal Test Report of the MPIfR, 1973).

3. Point Sources

The point sources visible in Fig. 1 are collected in Table 1. Only those point sources indicated by at least 2 contours ($\simeq 6\sigma = 0.10$ Jy/beam) above the immediate surrounding were included. The positional accuracy is estimated to be $\pm 4^s$ in α and $\pm 1'$ in δ. The random error in the flux density is about ± 0.05 Jy down to the weakest sources; the flux density scale is probably accurate to 10%.

We have compared the sources in Table 1 with an updated version of the Masterlist of Radio Sources (Dixon, 1970). Four-

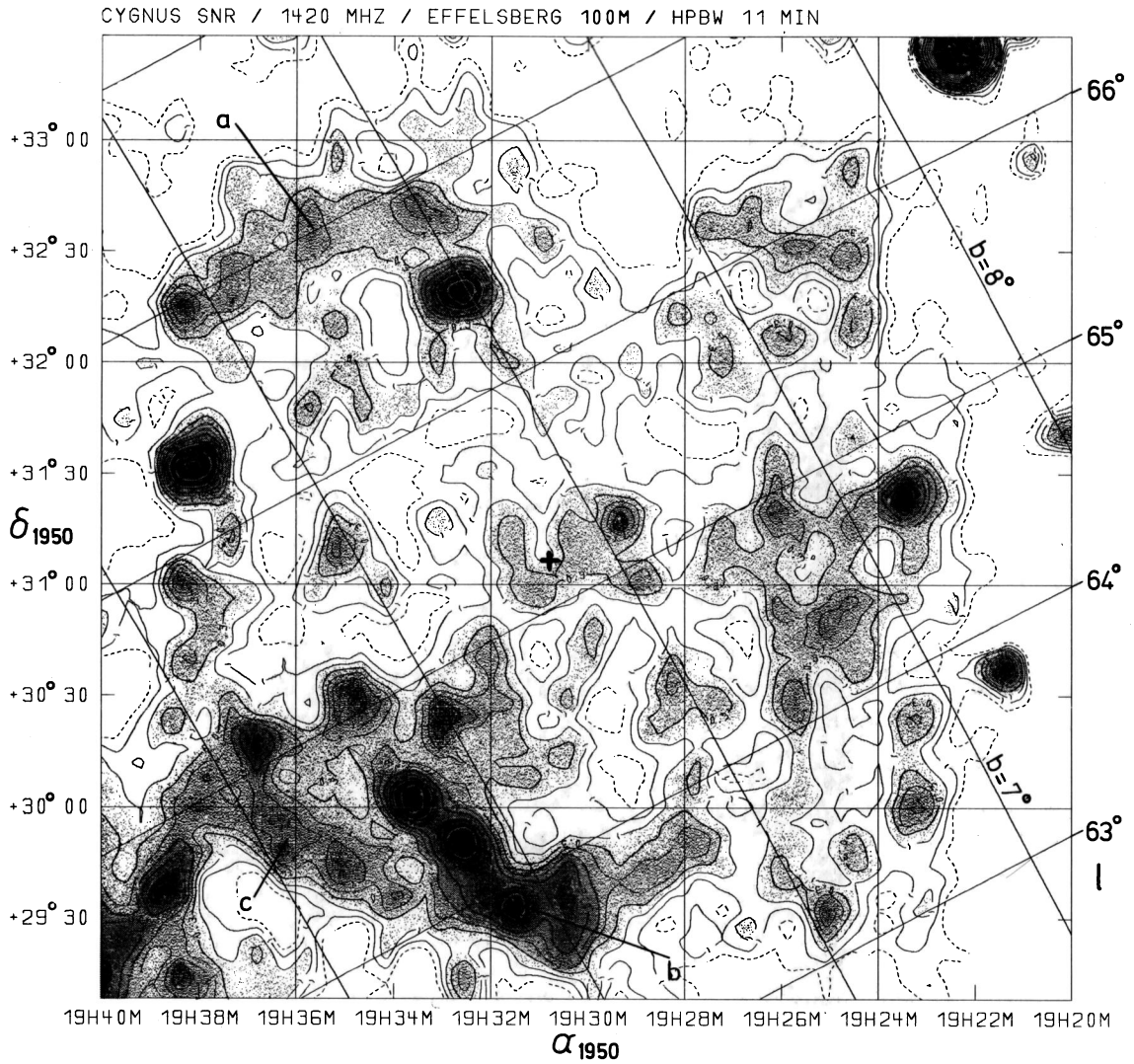

Fig. 1. Contour map of G65.2+5.7 at 1420 MHz smoothed to an angular resolution of 11′. Contour levels are 0 (dashed) step 0.1 K in main beam brightness temperature T_b; contours 0.3 and 0.6 K are thick. Areas where $T_b > 0.2$ K are blackened proportional to T_b. The r.m.s. noise is 0.03 K. Ridges *a*, *b*, and *c* are indicated (Sect. 4); + shows the position of the radio centre (Sect. 5)

teen sources, all of them having $S_{1420} \leqq 0.22$ Jy, do not appear in the Masterlist. One of them is the Sharpless H II region S94 (source 13 in Table 1), which has been detected at 1400 MHz by Felli and Churchwell (1972). Also at the position of S96 ($\alpha = 19^h27^m$, $\delta = 32°35'$) some enhanced emission is seen. Curiously, Felli and Churchwell (1972) using the 92-m telescope of NRAO did not detect any emission above 0.3 K in T_b, corresponding to 0.17 Jy/beam, in the part of our map between $\delta = 31°40'$ and $\delta = 33°00'$ where we see several sources above this level. The flux densities of known sources in Table 1 generally agree to within the errors with the values at the same frequency in the Masterlist.

It is interesting to see whether any enhancement of the number of point sources exists in this area. Wall et al. (1971) did source counts at 2700 MHz using the Parkes telescope with a half-power beamwidth of 10′, which is very close to the angular resolution of our map. Assuming an average spectral index of 0.75 between 1420 and 2700 MHz, the expected number of sources N ($S_{1420} \geqq 0.16$ Jy) is 15 ± 4, while 15 ± 5 sources are observed. The expected number of sources N ($S_{1420} \geqq 0.52$ Jy) is 3 ± 2, and 3 ± 1 sources are observed. So the number of sources observed in the area agrees very well with the expected number. However, in the strip of $0.^\circ3 \times 1.^\circ0$ centred at $\alpha = 19^h33^m$, $\delta = 29°50'$ on one of the bright radio ridges coincident with an optical filament we observe 3 ± 1 sources with $S_{1420} \geqq 0.16$ Jy, but only 0.23 ± 0.05 sources are expected. This suggests that some of the sources observed in this ridge may be physically related to the ridge. It may be noted that in several SNRs (Cygnus Loop, Origem Loop) point sources occur in the radio shell.

4. Comparison of the Map at 1420 MHz with Optical Observations

In Figure 1 several elongated structures or ridges stand out clearly, i.e. (a) in the north from $\alpha = 19^h32^m$ to 19^h39^m at $\delta \simeq 32°30'$, (b) in the south from $\alpha = 19^h28^m$ to 19^h34^m at $\delta \simeq 29°45'$, and (c) from $\alpha = 19^h34^m$ to 19^h37^m at $\delta \simeq 29°50'$.

In Figure 2 the contour map of Fig. 1 is superimposed onto the twenty-minute exposure in [O III] of Gull et al. (1977). The bright radio ridges appear to coincide with the brightest optical

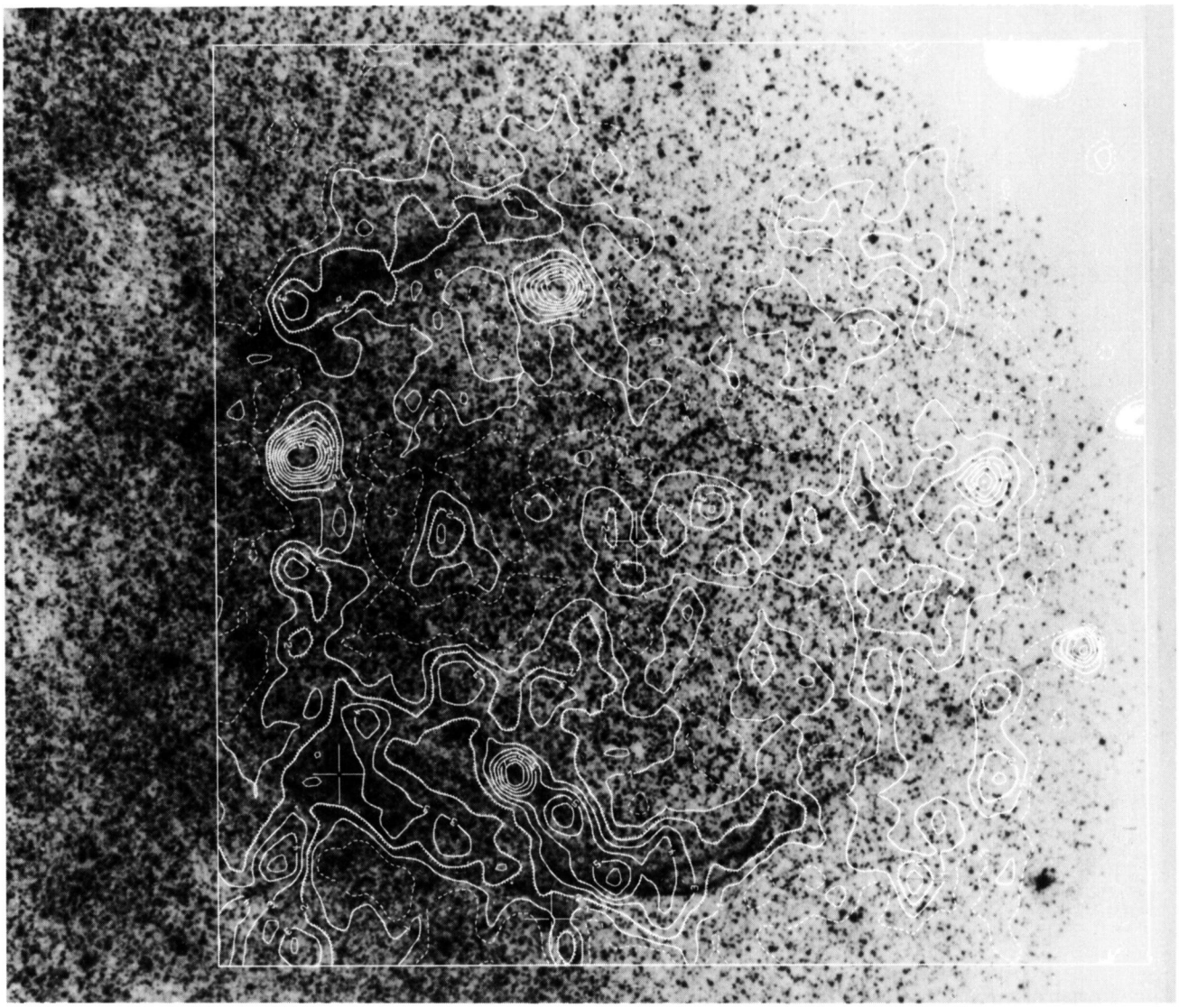

Fig. 2. Contour map of G65.2+5.7 at 1420 MHz with an angular resolution of 11′ superimposed onto the twenty-minute exposure in [O III] of Gull et al. (1977). Contours 0 (dashed) step 1 correspond to levels 0.05 K step 0.15 K in T_b; contour 2 is hatched downhill

filaments. This suggests that the shell of the SNR emits both optical and radio emission from gas of high density at high temperature as well as synchrotron emission from high-energy electrons in a possible compressed magnetic field (see Sect. 5). The patchiness of the radio ridges and the point sources in ridge *b* are reminiscent of the Cygnus Loop.

In addition to the bright ridges a small radio ridge coincides with the small but bright filament S94 at $(\alpha, \delta) = (19^h26^m, +31°20')$. On the weaker filaments no radio emission has been detected, putting an upper limit to the brightness temperature $T_b(1420) \lesssim 100$ mK. The radio ridge centred at $\alpha = 19^h39^m$, $\delta = 29°30'$ is probably a contamination of galactic plane emission unrelated to the SNR, which influences the map at the lowest latitudes.

5. Distribution of Spectral Index between 1420 and 408 MHz

In order to determine the spectral index distribution across the SNR the same area as observed at 1420 MHz was taken from the 408 MHz survey of Haslam et al. (1974). To separate the SNR emission from the background the baselevel of the map at 408 MHz was determined in the same way as at 1420 MHz. The full beam brightness temperatures were then multiplied by 1.5 in order to obtain main beam brightness temperatures. Using a gaussian function the map at 1420 MHz was smoothed to the half-power beamwidth of 37′ at 408 MHz. The temperature spectral index β was then computed for all temperatures larger than 4 times the r.m.s. noise, i.e. for points having $T_b(408) > 3$ K and $T_b(1420) > 0.1$ K. The result is shown in Fig. 3 superposed onto the contour map at 408 MHz. The estimated systematic error in β is ± 0.2, but may be higher at $\alpha > 19^h36'$ because of uncertainties in the baselevels. The random error due to noise in the maps is typically $0.6/T_b(408)$ per beam area.

In view of the above uncertainties an interpretation of Fig. 3 should be made with caution. For instance, ridge a in the north has $\beta = 2.30 \pm 0.12$, only marginally different from $\beta = 2.50 \pm 0.05$ of ridge b. Several sources have a steeper spectrum than their surroundings.

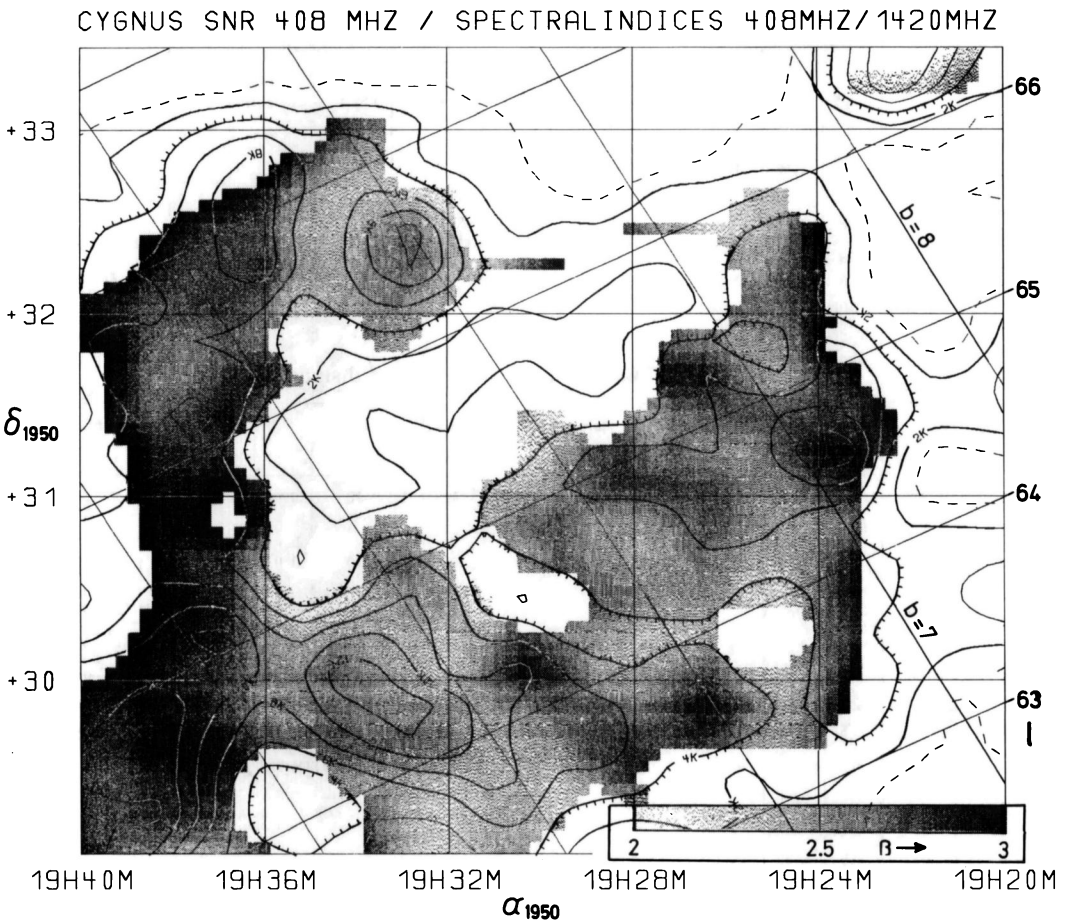

Fig. 3. Distribution of the temperature spectral index β_{1420}^{408} across G65.2+5.7 superimposed onto the 408 MHz map taken from Haslam et al. (1974). Contours are labelled in K in T_b; the contour of 4 K is hatched downhill. β_{1420}^{408} was determined only at positions where both $T_b(1420) > 0.01$ K and $T_b(408) > 3$ K hold. The random error in β_{1420}^{408} is $0.6/T_b(408)$

The average variation of β as a function of distance from the centre was also studied. The position of the centre and the ellipticity of the loop-like structure were estimated from the lines of maximum intensity of the radio ridges in Fig. 1. The centre is at $(\alpha, \delta) = (19^h30^m48 \pm 30^s, +31°5 \pm 2')$, or $(\ell, b) = (65°17 \pm 0.03, +5°73 \pm 0.03)$, and is indicated in Fig. 1; the axial ratio is 1.3 ± 0.1. For both maps the brightness temperatures were averaged in elliptical rings around the centre (now all points were used). The resulting cross-cuts and the average β are shown in Fig. 4. Apart from some emission near the centre the cross-cuts have the shape typical for SNRs: a relative minimum around the centre, a slow increase to maximum intensity, followed by a steep decrease from the maximum outwards. The emission near the centre is partly due to source 15 (Table 1); no optical counterpart is visible in Fig. 2. The average spectral index appears to slowly increase from $\beta = 2.34 \pm 0.14$ within 24′ from the centre to $\beta = 2.64 \pm 0.02$ at $R = 120'$ and $\beta = 2.96 \pm 0.04$ at $R = 150'$. However, the increase in β for $R > 120'$ is based on the uncertain outer parts of the maps. If the area $\alpha > 19^h36^m$ is left out then the increase of β for $R > 120'$ is somewhat less. The steepening of the spectrum from $R = 0'$ to $R = 120'$ is probably real.

6. Integrated Flux Density and Linear Diameter; Dynamical Model

Following Clark and Caswell (1976) the boundary of the elliptically shaped SNR was taken at $R = 156'$ along the "major axis" corresponding to $R = 120'$ along the "minor axis". The maps at 1420 and 408 MHz were integrated out to this radius yielding the integrated flux densities given in Table 2. The errors quoted in Table 2 are mainly due to uncertainty in the ellipticity; they do not include the uncertainties in the baselevels of the maps. The integrated flux density spectral index is $\alpha_{1420}^{408} = 0.61 \pm 0.05$ (but ± 0.25 if the systematic error is included).

The average surface brightness Σ was derived from the average brightness temperature T_b using the relation $\Sigma = 2k\bar{T}_b/\lambda^2$. Interpolation to 1000 MHz gives $\Sigma_{1000} = (1.46 \pm 0.05)\ 10^{-22}$ W m^{-2} sterad^{-1} Hz^{-1}. Σ_{408} and Σ_{1000} may be used to find the linear diameter D from the $\Sigma - D$ relation.

The $\Sigma - D$ relation is of the form $\Sigma = aD^{-b}$. The constants a and b have been determined by various authors using different, but partly identical, sets of calibrators. Applying the four most recent determinations to the new SNR, taking an average angular diameter of $276' = 4°6$, the values for the linear diameter D and distance r as listed in Table 3 are obtained. In view of the large uncertainties we adopt $D = 75^{+50}_{-25}$ pc and $r = 0.9^{+0.6}_{-0.3}$ kpc. These values confirm the estimates of Gull et al. (1977) (see Sect. 1). The agreement with the optically determined values of Sabbadin and D'Odorico (1976) is also reasonable; it may be noted that the relations they used show a considerable scatter, and that they observed line ratios only in one small part of the filaments indi-

Table 1. Sources in the region of SNR G65.2+5.7

Nr.	(1950) RA	(1950) DEC	S_{peak} (Jy)	Comments	Other names	Freq. (MHz)	S (Jy)	α^{ν}_{1420}
1	$19^h20^m00^s$	31°41'	0.29	upper limit for RA	4C+31.53	179	2.1	1.05
					B2 1919+31B	408	1.68	0.72
					OV+333	1415	0.19	-
2	19 20 50	32 56	0.16		B2 1920+32	408	0.37	0.68
3	19 21 20	30 36	0.45		4C 30.37	179	3.1	1.07
					B2 1921+30	408	1.68	0.95
					VRO 30.19.03	610	0.9	1.22
					OV 336	1415	0.37	-
4	19 22 24	33 25	3.55	used for calibration	4C 33.48	179	7.2	0.34
					B2 1922+33	408	7.24	0.57
					OV+337	1415	3.61	-
					DA 480	1420	2.9	-
					GC 1922+33	5000	1.92	0.49
5	19 23 12	30 00	0.19		B2 1923+29	408	0.51	0.81
6	19 23 14	30 24	0.16		-			
7	19 23 28	31 24	0.39		B2 1923+31	408	0.82	0.60
					OV+339	1415	0.58	-
8	19 24 30	32 10	0.16		-			
9	19 24 32	29 48	0.13		-			
10	19 24 39	32 28	0.14		B2 1924+32B	408	0.41	0.86
11	19 25 04	29 32	0.26		B2 1924+29	408	0.56	0.63
					OV+242	1415	0.28	-
12	19 25 56	32 08	0.16		B2 1925+32A	408	0.30	0.50
13	19 26 07	31 20	0.13	HII region	S94			
14	19 28 52	31 02	0.14		B2 1928+31	408	0.47	0.97
15	19 29 21	31 17	0.23		B2 1929+31	408	0.39	0.46
					OV+349	1415	0.22	-
16	19 29 53	30 48	0.12		-			
17	19 30 56	32 26	0.13		-			
18	19 31 05	30 58	0.13		-			
19	$19^h31^m28^s$	29°32'	0.18	extended background	-			
20	19 32 32	29 13	0.22		-			
21	19 32 32	29 50	0.17	extended background	B2 1932+29	408	0.89	1.32
					OV+254	1415	0.43	-
22	19 32 36	32 19	0.59	extended in RA	4C 32.60	179	3.3	0.83
					B2 1932+32	408	2.16	1.04
					OV+355	1415	0.36	-
23	19 32 58	30 24	0.14	Planetary nebula	PK064+5.1	3240	0.47	-
					"	6630	0.63	-
					"	10630	0.54	-
24	19 33 36	30 02	0.49		4C+29.58	179	3.9	1.00
					B2 1933+30	408	1.87	1.07
					VRO 29.19.01	610	0.9	0.72
					OV+356	1415	0.58	-
25	19 34 44	30 28	0.16		-			
26	19 35 09	31 10	0.16		B2 1935+31	408	0.37	0.67
27	19 35 45	31 48	0.13		-			
28	19 36 48	30 17	0.14		B2 1936+30	408	0.29	0.58
29	19 37 24	31 13	0.15		-			
30	19 38 08	31 32	0.70	extended in RA	B2 1938+31	408	1.38	0.54
					OV+364	1415	0.84	-
31	19 38 20	31 00	0.18		B2 1938+30	408	0.46	0.75
32	19 38 21	29 14	0.15		-			
33	19 38 24	32 16	0.16		-			
34	19 38 43	29 37	0.20		B2 1938+29	408	0.88	1.19

Estimated random errors: RA $\pm 4^s$, DEC $\pm 1'$, S_{peak} ± 0.05 Jy

Table 2. Integrated flux and surface brightness

ν (MHz)	S_{int} (Jy)	$\bar{T}_b$ (K)	Σ (10^{-22} W m^{-2} ster^{-1} Hz^{-1})
408	91 ± 5	4.93 ± 0.13	2.52 ± 0.07
1420	42.4 ± 1.6	0.19 ± 0.01	1.19 ± 0.04

Systematic errors are not included

Table 3. Linear diameter and distance

Reference	ν (MHz)	a	b	D (pc)	r (kpc)
Clark, Caswell (1976)	408	3.6×10^{-5}	10 ± 1	52^{+28}_{-16}	$0.6^{+0.4}_{-0.2}$
Ilovaisky, Lequeux (1972)	1000	4.55×10^{-15}	4.0 ± 0.2	74^{+19}_{-13}	$0.9^{+0.3}_{-0.1}$
Sabbadin (1977)	408	1.5×10^{-16}	3.0 ± 0.3	84^{+40}_{-20}	$1.0^{+0.5}_{-0.2}$
Berkhuijsen (1973)	1000	4.5×10^{-16}	3.1 ± 0.3	124^{+144}_{-45}	$1.5^{+1.8}_{-0.5}$
Adopted				75^{+50}_{-25}	$0.9^{+0.6}_{-0.3}$

The linear diameter was derived from $\Sigma_\nu = a D^{-b}$

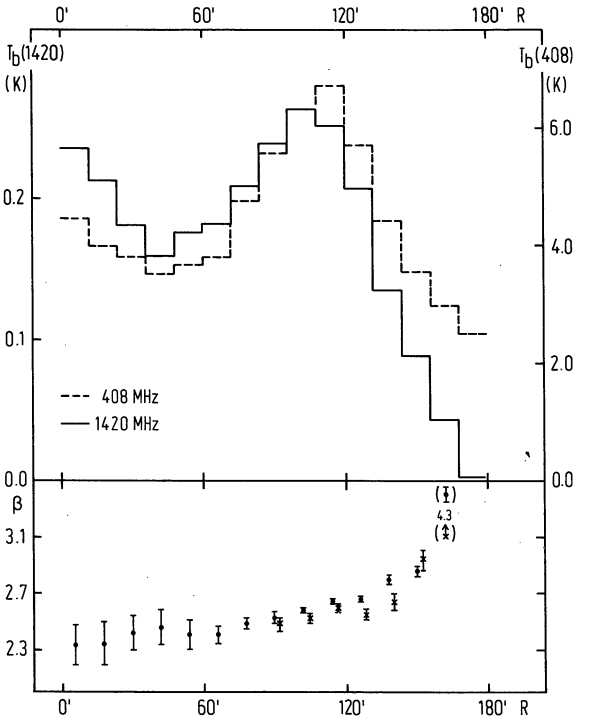

Fig. 4 a. Distribution of $T_b(1420)$ and $T_b(408)$ after averaging in elliptical rings around the centre at distance R from the centre. **b** Variation of the temperature spectral index β^{408}_{1420} with R derived from the data shown in Fig. 4a. Dots – entire area was used; crosses (slightly shifted for clarity) – area $\alpha > 19^h36^m$ not used. Error bars of one standard deviation are shown

Table 4. Data on SNR G65.2+5.7

Coordinates of centre		
optical shell	α (1950) (h,m)	19 31
	δ (1950) (°,')	+31 10
	ℓ (°)	65.6
	b (°)	+6
radio shell	α (1950) (h,m,s)	19 30 48±30
	δ (1950) (°,')	31 5±2
	ℓ (°)	65.17± 0.03
	b (°)	5.73± 0.03
Diameter of optical shell	D_o (°)	3.3 x 4.0
Diameter between outer half-power points of radio shell	D (°)	4.0 x 5.2
Axial ratio of radio shell		1.3 ± 0.1
Integrated flux density at 1 GHz	S_{int} (Jy)	52 ± 3
Flux density spectral index ($S \propto \nu^{-\alpha}$)	α_{1420}^{408}	0.61± 0.25
Average brightness temperature at 1 GHz	$\bar{T}_b$ (K)	0.48± 0.03
Average surface brightness at 1 GHz	Σ_{1000} (10^{-22} W m^{-2} ster^{-1} Hz^{-1})	1.46± 0.05
Average surface brightness at 408 MHz	Σ_{408} (10^{-22} W m^{-2} ster^{-1} Hz^{-1})	2.52± 0.07
Linear diameter of radio shell	D (pc)	75^{+50}_{-25}
Distance to centre of radio shell	r (kpc)	$0.9^{+0.6}_{-0.3}$
Distance above Galactic plane	z (pc)	90^{+60}_{-30}
Expansion velocity	V_{exp} (km/s)	$\gtrsim 50$
Age	t (10^5 years)	$\lesssim 2.4^{+1.4}_{-0.8}$
Assumed ambient magnetic field	B_o (10^{-6} Gauss)	3
Ambient density	n_o (cm^{-3})	9^{+21}_{-7}
Initial energy	E_o (10^{51} ergs)	13 ± 2

cative for the shell. Observations of the line ratios in other parts of the shell are highly desirable.

Gull et al. (1977) have noted that the expansion velocity $V_{exp} \gtrsim 50$ km s^{-1} in order to produce the observed strong [O III] lines. From the values of $I(H\alpha)/I(N II)$ observed in S91 Sabbadin and D'Odorico (1976) estimated $V_{exp} \gtrsim 100$ km s^{-1}. However, Lozinskaya (1978) has shown that within old SNRs the expansion velocity of filaments can range from 0 to 150 km/s. Therefore, the value of V_{exp} derived for S91 may not be typical for the new SNR as a whole and we adopt $V_{exp} \gtrsim 50$ km s^{-1}. With a linear diameter $D = 75^{+50}_{-20}$ pc we then find an age $t \lesssim 2.4^{+1.4}_{-0.8}\ 10^5$ yr and a ratio of total kinetic energy to ambient density $E_o/n_o^{1.12} \gtrsim 1.1^{+2.0}_{-1.0}\ 10^{51}$ erg cm$^{-3.36}$ (Chevalier, 1974).

Recently Cantó (1977) derived an empirical relation between linear radius, n_o and V_{exp} for the case of a magnetic field $B_o = 3\ 10^{-6}$ Gauss. Since we observed nonthermal radio emission from the remnant this case may be applicable. Using his Fig. 3 we find $n_o \lesssim 9^{+21}_{-7}$ cm^{-3} yielding $E_o \sim (13 \pm 2) \times 10^{51}$ erg. This energy is ~3 times the average E_o of about 20 SNRs obtained by Cantó.

7. Summary and Discussion

The results of our observations at 1420 MHz with an angular resolution of 11′ (Fig. 1) of the new SNR G65.2+5.7 that has been detected optically by Gull et al. (1977) may be summarised as follows:

1. At 1420 MHz several intense radio ridges are found coinciding with the brightest optical filaments. Most of the weaker filaments are not seen at 1420 MHz giving an upper limit of $T_b < 100$ mK (Fig. 2). A cross-cut through the object obtained by averaging T_b in rings around the centre has a shape typical for SNRs (Fig. 4).

2. Comparison with existing data at 408 MHz of Haslam et al. (1974) shows the existence of variation in the temperature spectral index β between 2.3 and 2.9 (Fig. 3). After averaging T_b in rings a systematic increase in β is found from $\beta = 2.34 \pm 0.14$ at $R < 24'$ to $\beta = 2.64 \pm 0.02$ at $R = 120'$ (Fig. 4). For $R < 156'$ the integrated spectral index is 2.61 ± 0.25 indicating that the radiation at 1420 MHz is mainly nonthermal.

3. The observed and derived parameters of the new SNR are collected in Table 4. Its main characteristics are: $D \simeq 75$ pc, $r \simeq 0.9$ kpc, $V_{exp} \gtrsim 50$ km s^{-1}, $t \lesssim 2.4\ 10^5$ yr, and $E_o \simeq 13 \times 10^{51}$ erg if $n_o \lesssim 10$ cm^{-3}.

In Table 5 G65.2+5.7 is compared with other SNRs of large size and low radio brightness. The linear diameter and radio surface brightness of G65.2+5.7 are intermediate between those of the Monoceros Loop and S147 and those of the Origem Loop, but the optical appearance, expansion velocity and age are close to those of S147 and the Monoceros Loop. Therefore, G65.2+5.7 seems to be most comparable to these younger remnants, optically in particular to S147; it is larger than S147 mainly because of its larger initial energy.

The values of n_o were derived from Fig. 3 in Cantó (1977) using the values of V_{exp} from Table 5. The ambient densities come out a factor of ~10 higher than is usually assumed. Unfortunately independent observations of n_o in the directions of the 4 SNRs in Table 5 are scarce. Raimond (1964) found evidence for extended H I complexes having densities of ~10 cm^{-3} in the direction and at the approximate distance of the Monoceros Loop. Considering that most probably H_2 is also present in these clouds, as well as the fact that supernovae are likely to explode in relatively dense regions, an ambient density $n_o \simeq 10$ cm^{-3} may be more realistic than $n_o \simeq 1$ cm^{-3}. Consequently, the typical initial kinetic energy that is usually assumed also increases by a factor of ~10 to $\simeq 3 \times 10^{51}$ erg.

Finally, the observations of G65.2+5.7 presented here clearly demonstrate that extended SNRs of low radio surface brightness not only can be detected, but also can be separated from a fairly complex Galactic background, provided the radio observations are done with sufficiently high resolution (HPBW $\lesssim 10'$) at a suitable frequency ($\lesssim 1400$ MHz). Detailed optical surveys (Gull et al., 1974) as well as H I surveys with high resolution will greatly improve the chance of finding weak extended SNRs. Therefore we believe that, contrary to the conclusion of Henning and Wendker (1975), many more extended SNRs having $\Sigma_{408} \gtrsim 1.5$ 10^{-22} W m^{-2} sterad^{-1} Hz^{-1} may be detected in the future.

References

Bergh, S. van den, Marscher, A. P., Terzian, Y.: 1973, *Astrophys. J. Suppl.* **26**, 19
Berkhuijsen, E. M.: 1972, *Astron. Astrophys. Suppl.* **5**, 263
Berkhuijsen, E. M.: 1973, *Astron. Astrophys.* **24**, 143

Table 5. Comparison of G65.2+5.7 with similar SNRs

Variable	Monoceros Loop	S147	G65.2+5.7	Origem Loop	References
Optical appearance	faint HII ring weak filaments	shell of long filaments	shell of long filaments, strong [OIII/Hα]	some bright HII regions, no filaments	1,1,4,6
ℓ,b (°)	205.5, +0.2	180.0, -1.7	65.2, +5.7	194.7, +0.4	2,2,7,6
$\Sigma_{408}(10^{-22}$ W m^{-2} ster^{-1} Hz$^{-1})$	4.1 ± 0.4	5.2 ± 0.5	2.5 ± 0.1	2.2 ± 0.5	2,2,7,6
D (pc)	49 ± 10	51 ± 10	75^{+50}_{-25}	116 ± 52	2,2,7,6
r (kpc)	0.7 ± 0.2	1.0 ± 0.2	$0.9^{+0.6}_{-0.3}$	1.1 ± 0.5	2,2,7,6
V_{exp} (km/s)	50 ± 10	50 ± 10	$\gtrsim 50$	~ 20	3,3,4,6
t (10^5 years)	1.5 ± 0.4	1.5 ± 0.4	$\lesssim 2.4^{+1.4}_{-0.8}$	~ 10	8,8,8,8
$E_o/n_o^{1.12}$ (10^{51} erg cm$^{-3.36}$)	0.3 ± 0.2	0.3 ± 0.2	$\gtrsim 1.1^{+2.0}_{-1.0}$	~ 1	8,8,8,8
n_o (cm^{-3})	14^{+22}_{-12}	12^{+19}_{-10}	$\lesssim 9^{+21}_{-7}$	~ 0.5 [~ 6]	9,9,7,6 [9]
E_o (10^{51} erg)	5 ± 1	5 ± 1	13 ± 2	~ 0.5 [~ 6]	

(1) van den Bergh et al. (1973); (2) Clark, Caswell (1976); (3) Lozinskaya (1978); (4) Gull et al. (1977); (5) Sabbadin, D'Odorico (1976); (6) Berkhuijsen (1974); (7) this paper; (8) derived from $0.3\ R = V_{exp}\ t\ 10^6$ pc and $E_o\ 10^{50} = 5.3\ 10^{-7}\ n_o^{1.12}\ V_{exp}^{1.4}\ R^{3.12}$ ergs, both holding after the shell has been formed (Chevalier, 1974); (9) Cantó (1977), Figure 3; a magnetic field of 3×10^{-6} Gauss has been assumed.

Berkhuijsen, E. M.: 1974, *Astron. Astrophys.* **35**, 429

Cantó, J.: 1977, *Astron. Astrophys.* **61**, 641

Chevalier, R. A.: 1974, *Astrophys. J.* **188**, 501

Clark, D. J., Caswell, J. L.: 1976, *Monthly Notices Roy. Astron. Soc.* **174**, 267

Daltabuit, E., D'Odorico, S., Sabbadin, F.: 1976, *Astron. Astrophys.* **52**, 98

Dixon, R. S.: 1970, *Astrophys. J. Suppl.* **20**, 1

Felli, M., Churchwell, E.: 1972, *Astron. Astrophys. Suppl.* **5**, 369

Genzel, R., Pauliny-Toth, I. I. K., Witzel, A.: 1976, Interner Bericht des MPIfR Nr. 30

Gull, T. R., Kirshner, R. P., Parker, R. A. R.: 1977, *Astrophys. J.* **215**, L69

Haslam, C. G. T., Wilson, W. E., Graham, D. A., Hunt, G. C.: 1974, *Astron. Astrophys. Suppl.* **13**, 359

Henning, K., Wendker, H. J.: 1975, *Astron. Astrophys.* **44**, 91

Ilovaisky, S. A., Lequeux, J.: 1972, *Astron. Astrophys.* **18**, 169

Lozinskaya, T. A.: 1978, *Astron. Astrophys.* **64**, 123

Neidhöfer, J., Wilson, W., Haslam, C. G. T.: 1978, *Kleinheubacher Berichte* **21**, 215

Raimond, E.: 1964, Ph. D. Thesis, Leiden University.

Sabbadin, F.: 1977, *Astron. Astrophys.* **54**, 915

Sabbadin, F., D'Odorico, S.: 1976, *Astron. Astrophys.* **49**, 119

Sharpless, S.: 1953, *Astrophys. J.* **118**, 362

Wall, J. V., Shimmins, A. J., Merkelijn, J. K.: 1971, *Australian J. Phys. Suppl.* **19**, 1